Available online at www.sciencedirect.com
SCIENCE DIRECT®
Journal of Solid State Chemistry 177 (2004) 1758–1767
JOURNAL OF SOLID STATE CHEMISTRY
http://elsevier.com/locate/jssc

Structural study of $(U_{0.90}Ce_{0.10})_4O_{9-\delta}$, an anion-excess fluorite superstructure of $U_4O_{9-\delta}$ type

C. Rocanière,[a] J.P. Laval,[b,*] Ph. Dehaudt,[c] B. Gaudreau,[b] A. Chotard,[d] and E. Suard[e]

[a] *Commissariat à l'Energie Atomique, CEA Grenoble, Avenue des Martyrs, 38 Grenoble, France*
[b] *Science des Procédés Céramiques et de Traitements de Surface, UMR-CNRS No. 6638, 123, Avenue A. Thomas, 87060 Limoges Cedex, France*
[c] *Commissariat à l'Energie Atomique, CEA Saclay, DEN/DSNI, Bât 121, 91191 Gif sur Yvette, France*
[d] *Framatome-ANP Combustible Nucléaire, 10 rue J. Récamier, 69456 Lyon Cedex 06, France*
[e] *Institut Laüe-Langevin, B.P. 156, 38042 Grenoble Cedex 9, France*

Received 10 September 2003; received in revised form 23 December 2003; accepted 30 December 2003

Abstract

In the U–Ce–O system, a solid solution $(U,Ce)O_{2+x}$ of fluorite type containing anionic excess is known in a wide composition range. For high values of x, it transforms to a $(U_{1-y}Ce_y)_4O_{9-\delta}$ phase deriving from the β-$U_4O_{9-\delta}$ type [ordered anion-excess fluorite superstructure phase; I-43d space group; $a = 21.7484(1)$ Å for $y = 0.10$]. The crystal structure of $(U_{0.9}Ce_{0.1})_4O_{9-\delta}$ has been refined by the Rietveld method on a powder sample measured on D2B at ILL Grenoble. The structural model, proposed by Bevan et al. for β–$U_4O_{9-\delta}$ and not fully confirmed till now, has been verified. The structure is based on an ordered distribution of cuboctahedral clusters U_6O_{37} inside a fluorite matrix. A preferential ordering of Ce^{4+} (and U^{4+}) on the so-called "centaur polyhedra" with 10 coordination is proposed, on the basis of bond valence calculations. The structure so determined has the composition $M_{64}O_{143}$ ($MO_{2.234}$) and no traces of excess anions, completing the supposed composition up to M_4O_9, could be detected.

Keywords: Uranium oxide; Crystal structure; Neutron diffraction; Rietveld study; Fluorite structure; Defect structure

1. Introduction

While UO_2 fuels are the major components of light water reactors (LWR), most of them nowadays include other additive elements. *MOX* fuel, using Pu as fissile element, plays a major role in the fuel cycle. Gd-doped fuels are normally used in BWR (boiling water reactors) and sometimes in PWR (pressurized water reactors), in order to control the initial reactivity of the core. Er is expected as a new potential burnable absorber. Burning of long-life radioelements could take place as targets of these elements in a solid mixture with U.

Most of these additive elements form solid solutions of fluorite type. According to the oxygen potential range of UO_{2+x}, sintering in oxidizing atmosphere of these compounds as powders occurs at lower temperatures and can produce a more homogeneous material. It becomes important to improve our knowledge of the defect structure of these doped phases, which can present physical and structural features notably different from the pure uranium oxides.

In the present work, CeO_2, which is of particular interest with its two valences +3 and +4, able to simulate PuO_2 in solid solutions with uranium oxide, has been introduced in oxidizing atmosphere (CO_2) in order to produce $(U_{1-y}Ce_y)O_{2+x}$ fluorite solid solutions and $(U_{1-y}Ce_y)_4O_{9-\delta}$ ordered fluorite superstructures on pellet and powder samples and to determine their structure. The Ce content covers the range $y = 0-0.6$.

The phase diagram of the U–Ce–O system (O/U > 2.00), partly established by Markin [1], at temperatures ranging from 25°C to 600°C, shows, for compositions near the U–O system, three domains:

(i) A solid solution MO_{2+x} ($M = U_{1-y}Ce_y$) of fluorite structure, approximately delimited by the compositions $UO_{2.22}$, $U_{0.5}Ce_{0.5}O_{2.25}$, and CeO_2. Increasing y above 0.1 reduces the extent of the composition domain.
(ii) A $M_4O_{9-\delta}$ phase, supposed of the β-$U_4O_{9-\delta}$ type (superstructure of the fluorite type, of Fm-3m space

*Corresponding author. fax: +33-05-55-45-72-70.
E-mail address: laval@unilim.fr (J.P. Laval).

0022-4596/$ - see front matter © 2004 Elsevier Inc. All rights reserved.
doi:10.1016/j.jssc.2003.12.037

group, with lattice parameter $a = 4a_F$), although the presence of superlattice lines did not seem to have been determined. Its composition limits should be $2.2 < O/M < 2.25$ and become narrower for high Ce content.

(iii) Between these two phases, a biphased domain whose limits vary with temperature and Ce content.

For high oxidation degrees of U, the $M_4O_{9-\delta}$ phase coexists with an orthorhombic U_3O_8 (or M_3O_8) phase.

In the present work, the attention is focussed on the $M_4O_{9-\delta}$ domain for $y \leqslant 0.20$ mol Ce and especially on the structural description of $(U_{0.9}Ce_{0.1})_4O_{9-\delta}$, studied by mean of neutron powder diffraction data.

2. Experimental

The $U_4O_{9-\delta}$ and $(U_{1-y}Ce_y)_4O_{9-\delta}$ phases are synthesized following successive steps:

homogeneous mixtures of $UO_{2.15}$ and CeO_2 powders are prepared by ball milling, during 4 h, of samples of 100 g in presence of 1 kg uranium bullets (instead of steel or ceramics bullets to prevent contamination of the powders, critical for nuclear fuels). Then, the blended powders are pressed at 500 MPa giving pellets of 7 g.

The reactions of homogenization are realized by a thermal treatment in a sintering furnace under CO_2 atmosphere (< 10 vpm O_2), with successively: 20 h at 1200°C, 30 h at 1300°C and 30 h at 1200°C. The heating and cooling speed are 600°C/h.

After all thermal treatments, the final O/M ratio is controlled by weight loss of samples after and before heating and by comparison with thermogravimetric (TGA) experiments under the same CO_2 atmosphere (SETARAM TG-85-16-18). The moisture loss of powders and the deviation of the thermobalance during heating are corrected. Moreover, a calibration with a sample of UO_{2+x} heated in the same furnace, allows to compare the O/U ratio determined from weight loss after and before heating and after reduction in UO_2 under H_2. The difference Δ(O/U) has been used to calibrate the measurements on the samples heated in the sintering furnace. The accuracy estimated on O/M is ± 0.02. It has also been verified that, under our synthesis conditions, the weight loss by evaporation of UO_3 is neglectible.

Under these standard conditions, the oxygen potential is -108 kJ/mol which corresponds to a partial pressure of oxygen of 15 P. For Ce-free samples, the composition in equilibrium under these conditions is always $UO_{2.20}$. Considering a formal reaction between $UO_{2.20}$ and CeO_2, which can be written:

$$(1-y)UO_{2.20} + yCe^{4+}O_2 \rightarrow (U_{1-y}Ce_y^{4+})O_{2+x'} + a/2O_2$$
$$\text{with } 0 \leqslant x' \leqslant 0.2$$

a slight loss of oxygen is evidenced as shown on the following table. An increase of the y content in Ce corresponds to a slight decrease of O/U and O/M ratios which are however greater than 2.00.

Evolution of O/M and O/U ratios after reaction under CO_2 atmosphere and loss of oxygen from the initial mixture.

yCe	O/M_{exp}	O/U_{exp}	Oxygen loss from initial mixture
0	2.20(1)	2.20	0
0.1	2.15(2)	2.16	0.01
0.2	2.12(2)	2.15	0.04
0.3	2.10(2)	2.14	0.04
0.4	2.07(2)	2.12	0.05
0.5	2.03(2)	2.06	0.05

After this homogenization process which gives products insufficiently oxidized for our purpose, the samples with $y = 0.1$ and 0.2 are reheated during 28 h at 1200°C under a mixture Ar + 10% air and cooled at 600°C/h under Ar atmosphere. After all these further thermal treatments under more oxidizing conditions, the final O/M composition is also controlled by weight loss and by comparison with TGA experiments under the same atmosphere. Electronic microprobe (EM) examination allows to verify the absence of Ce-rich aggregates. The final O/M ratio is, respectively, 2.26(2) and 2.17(2) for $y = 0.1$ or 0.2.

For $y = 0.3-0.6$, the best treatment to obtain high values of O/M without formation of U_3O_8 occurs under dry air and O/M ratio is very sensitive to temperature evolution: O/M increases as temperature T decreases.

A sample without Ce has also been prepared by heating $UO_{2.23}$ under Ar + traces of O_2 during 1 h at 1100°C, then 24 h at 700°C and cooling at 400°C/h to ambient temperature. Its final O/M composition, controlled by reduction under H_2, is 2.26.

The homogeneity of the reaction products and the lattice parameters of the phases are determined by X-ray diffraction on a Philips PW1380 diffractometer (Co$K\alpha$ reflection) equipped with a back-monochromator. The structural study used neutron diffraction measurements obtained on the D2B diffractometer at ILL ($\lambda = 1.593845$ Å) from 0° to 162.5° by 0.05° steps and count/step = 100,000. The samples were sintered pellets of 7 mm diameter fitted in a vanadium container.

3. Results

3.1. Characterization

3.1.1. $U_4O_{9-\delta}$ compound

The results of the synthesis agree with the previous works concerning the U–O system:

The "$UO_{2.20}$" sample with $O/M = 2.20$ is a mixture of two phases, a major phase $U_4O_{9-\delta 1}$ of sublattice parameter $a_F = 5.448_5$ Å and superlattice lines (only in agreement with the space group I-43d [2] ($a = 4 \times a_F = 21.794$ Å) and a minor phase of cubic symmetry whose lattice parameter $a_F = 5.469_2$ Å corresponds to $UO_{2.13}$.

The sample with $O/M = 2.26$ is a mixture of a major phase $U_4O_{9-\delta 2}$ with $a_F = 5.442_0$ ($a = 21.768$ Å) and of traces of: α-U_3O_{8-y}.

The lattice parameter of $U_4O_{9-\delta 2}$ agrees well with previous studies [3–6] for the upper limit in presence of U_3O_8. For the lower limit, the reported values can be different from an author to another which tends to show that this limit varies with the synthesis conditions (temperature and cooling rate).

The relative intensity of the weak lines characteristic of the superstructure increases from $U_4O_{9-\delta 1}$ to $U_4O_{9-\delta 2}$, in agreement with Ishii previous observations [5]. That likely indicates a progressive distortion of the U and O sublattices with the increasing O content. Moreover, the most intense superstructure lines (very weak on the X-ray diffraction pattern) are located at low angles, mainly about 50° (2θ). That appears to be in contradiction with Belbeoch and Lauriat [7,8] which observed the most intense superstructure lines at high angles and interpreted these features on the basis of slight ordered shifts of the cations by reference to UO_2 ideal structure. However, a true comparison with our results is made difficult because the measurements of these authors were performed on single crystals.

3.1.2. $(U_{1-y}Ce_y)_4O_{9-\delta}$ phase

- $y = 0.1$: The global composition resulting from analysis is $U_{0.9}Ce_{0.1}O_{2.26}$. The major phase obtained is an ordered phase with superlattice lines very similar to those of $U_4O_{9-\delta}$. It coexists with traces of α-U_3O_8 (or α-$(U,Ce)_3O_8$). The lattice parameter $a = 21.752_3$ Å $= 4a_F$ ($a_F = 5.438_1$ Å) is smaller than for $U_4O_{9-\delta}$, in agreement with the smaller radius of the Ce^{4+} cation (0.97 vs. 1.00 Å for U^{4+}). The composition of the major phase cannot be exactly determined but is very close to $(U_{0.9}Ce_{0.1})O_{2.25}$.
- $y = 0.2$: The global O/M ratio is lower: $O/M = 2.17$ and three phases are present. A small quantity of U_3O_8, (probably Ce-free because its lattice parameters are unchanged), a fluorite disordered solid solution of lattice parameter $a_F = 5.459_5$ Å (close to $U_{0.8}Ce_{0.2}O_{2.00}$ one: $a_F = 5.4582$ Å) and a major phase of $M_4O_{9-\delta}$ type with a lattice parameter $a = 21.776_4$ Å ($a_F = 5.444_1$ Å), higher than the previous ones, and then containing a lower anion excess, as attested by the lower intensity of the superlattice lines.
- $y = 0.3$: There is a complete disappearance of the superlattice lines of the observed fluorite phase. Thus, under our synthesis conditions, the $M_4O_{9-\delta}$ phase is not formed for $y > 0.2$ but it is not possible to definitively conclude about the limit of composition of this phase still observed by Markin for $y = 0.34$ [1]. It is possible that even more oxidizing conditions are necessary to stabilize this phase for high Ce contents.

3.2. Structure determination of β-$(U_{0.9}Ce_{0.1})_4O_{9-\delta}$

The structure of β-$U_4O_{9-\delta}$ has never been fully refined [8] and only a convincing structural model has been proposed by Bevan et al. [9]. It is supported by a theoretical stability calculation using the HADES code and by a partial structural determination [9,10]. This structural model is based on an ordered distribution, in the I-43d unit cell, of structural units called "cuboctahedral clusters", as shown in Fig. 1, coherently integrated within the fluorite matrix by substitution of anionic cubes O_8 by anionic cuboctahedra O_{12}. Each cluster consists in an octahedral arrangement of six UO_8 square antiprisms sharing corners (Figs. 1 and 2a) and

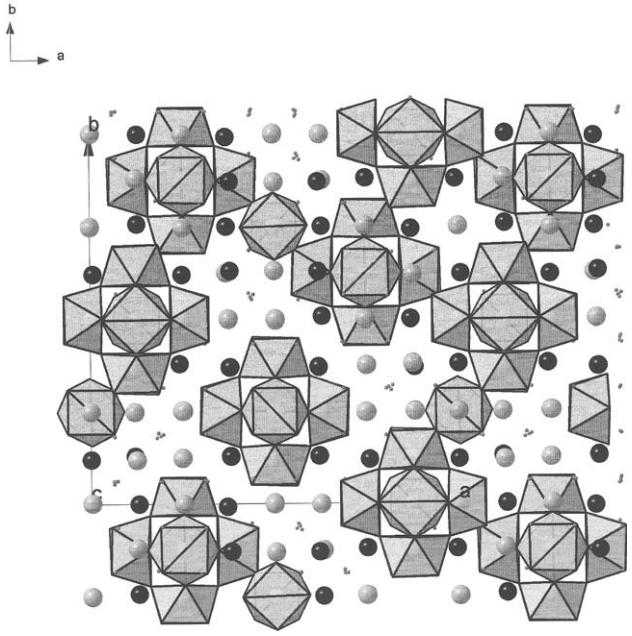

Fig. 1. Ordered distribution of cuboctahedral clusters in $(U_{0.9}Ce_{0.1})_4O_{9-\delta}$. For clarity, only the UO_8 square antiprisms of the cuboctahedral clusters are drawn and only three successive cationic layers are represented.

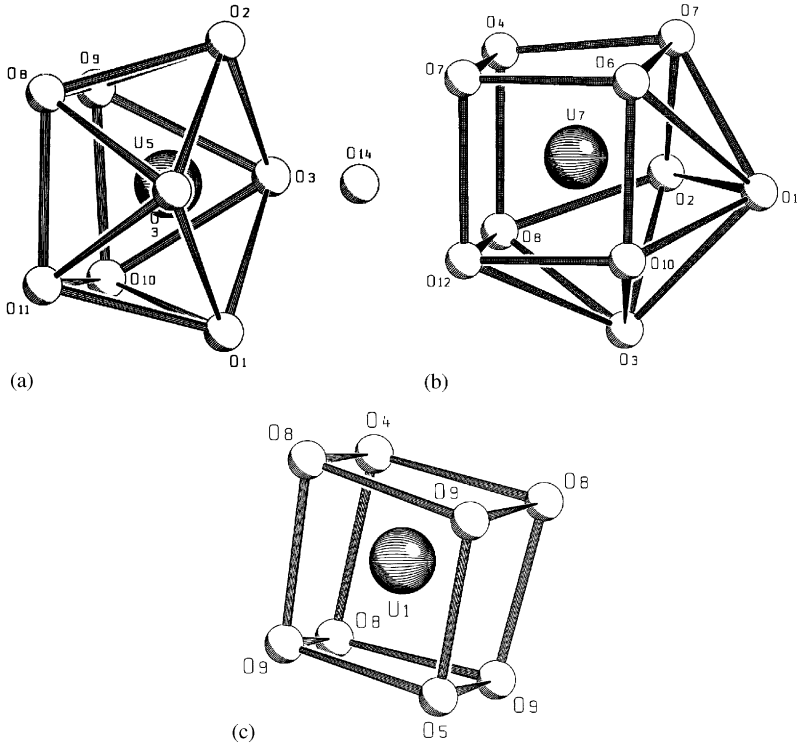

Fig. 2. (a): UO_8 square antiprism in $(U_{0.9}Ce_{0.1})_4O_{9-\delta}$ (b): U(Ce)O_{10} "centaur" polyhedron (half cube-half icosahedron) in $(U_{0.9}Ce_{0.1})_4O_{9-\delta}$ (c) UO_8 slightly distorted cube in$(U_{0.9}Ce_{0.1})_4O_{9-\delta}$.

eight "centaur" polyhedra UO_{10} (half cubes-half icosahedra: see Fig. 2b); UO_8 cubes (Fig. 2c) are located between the clusters. This structural process increases the anionic content but does not change the *fcc* cationic framework which is only slightly expanded near to the cluster. The anionic excess so accommodated corresponds to 4O for each cluster and even 5 if the inside of the anionic cuboctahedron is occupied by an extra O anion, weakly bonded to the cations as, e.g., in $Na_7Zr_6F_{31}$ [11], structure type adopted by many $M_7U_6F_{31}$ and $M_7Th_6F_{31}$ phases [12]. This model explains in a very elegant way the structural relationship between β-$U_4O_{9-\delta}$ and UO_2.

On the basis of this structural model and of neutron diffraction data obtained from a single crystal, Willis [10] has tried to estimate the displacements of the cations in the cluster by reference to UO_2, so retaining *m*-3*m* or -43*m* symmetry for the cluster (instead of -4 as resulting from the *I*-43*d* space group of β-$U_4O_{9-\delta}$). This constrained procedure removes the influence of the long-range cluster–cluster interaction and allows to lay emphasis on the small cationic and anionic shifts inside the cluster. It also allows to strongly reduce the number of independent parameters.

These results have been used to determine the complete structure of $(U_{0.9}Ce_{0.1})_4O_{9-\delta}$, in order to confirm the structure model of Bevan and the structural study of Willis and afterwards to analyze the U and Ce distribution on the different cationic sites. The structure refinement is performed with Fullprof code [13] and the neutron diffraction pattern measured with the D2B diffractometer (Fig. 3). The atomic coordinates are reported in Table 1 and their shift, by reference to the HADES model previously calculated [9], in Table 2.

3.3. Cationic sites

Contrary to the previous studies of Bevan [9], Willis [10] and Lauriat [8] which had used cationic sites either fixed at the ideal values deduced from the fluorite subcell or constrained, it has been attempted in the present work to freely refine their position in the way allowed by the *I*-43*d* space group. The cations move only slightly from these ideal positions as shown in Table 2. In agreement with Willis conclusions, the main shifts come from U_6 and U_7 cations inside centaur polyhedra which move inward toward the center of the anionic cuboctahedra. On the contrary, the U_4 and U_5 cations in square antiprisms slightly move outward. These movements are reflected in the U–U distances inside the cuboctahedral clusters, those between cations in square antiprisms and "centaur polyhedra", e.g., U_7–U_4 (3.677 Å) and U_7–U_5 (3.703 and 3.782 Å) being the shortest ones and the U_4–U_5 distances between cations in corner-shared square antiprisms being among the longest ones (3.897 and 3.894 Å).

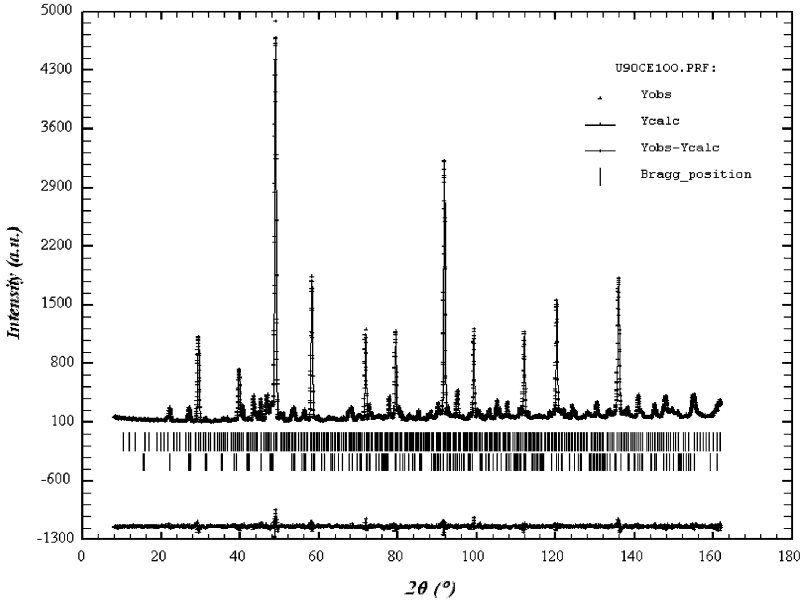

Fig. 3. Neutron diffraction pattern (experimental, calculated and difference) for $(U_{0.9}Ce_{0.1})_4O_{9-\delta}$.

Table 1
Refined structural parameters in the *I*-43*d* space group for $(U_{0.9}Ce_{0.1})_4O_{9-\delta}$ with Ce cations only located on the so-called "centaur "sites U_6 and U_7

Atom	Site	$(U_{0.9}Ce_{0.1})_4O_{9-\delta}$–$a = 21.7484(1)$ Å				
		x	*y*	*z*	*B* (Å^2)	τ
U_1	16*c*	0.0026(4)	0.0026(4)	0.0026(4)	0.16(6)	
U_2	24*d*	0.2516(8)	0	0.25	0.16(6)	
U_3	48*e*	0.1249(5)	0.1197(4)	0.2484(6)	0.16(6)	
U_4	24*d*	−0.0020(6)	0	0.25	0.62(9)	
U_5	48*e*	0.8749(5)	0.0031(4)	0.1198(4)	0.62(9)	
U_6	48*e*	−0.0053(5)	0.1223(6)	0.3711(5)	0.19(7)	0.72(6)
Ce_6	48*e*	−0.0053(5)	0.1223(6)	0.3711(5)	0.19(7)	0.28(6)
U_7	48*e*	−0.0017(6)	0.1199(4)	0.1308(5)	0.19(7)	0.79(6)
Ce_7	48*e*	−0.0017(6)	0.1199(4)	0.1308(5)	0.19(7)	0.21(6)
O_1	48*e*	−0.0287(7)	0.0935(7)	0.2549(7)	1.7(2)	
O_2	48*e*	−0.0325(5)	−0.0001(7)	0.3424(6)	0.60(2)	
O_3	48*e*	0.8771(7)	0.0962(5)	0.3438(6)	0.60(2)	
O_4	16*c*	0.0608(8)	0.0608(8)	0.0608(8)	0.60(2)	
O_5	16*c*	0.1817(7)	0.1817(7)	0.1817(7)	0.60(2)	
O_6	48*e*	0.0622(8)	0.1835(8)	0.1931(9)	0.60(2)	
O_7	48*e*	0.0731(9)	0.0619(7)	0.1879(7)	0.60(2)	
O_8	48*e*	−0.0635(8)	0.0631(7)	0.0554(7)	0.60(2)	
O_9	48*e*	−0.0664(7)	0.0594(7)	0.4521(6)	0.60(2)	
O_{10}	48*e*	−0.0604(7)	0.1978(7)	0.1891(8)	0.60(2)	
O_{11}	48*e*	−0.0609(6)	0.1954(9)	0.3145(7)	0.60(2)	
O_{12}	48*e*	0.0688(7)	0.0634(7)	0.3091(6)	0.60(2)	
O_{13}	48*e*	−0.0680(7)	0.1849(7)	0.4391(7)	0.60(2)	
O_{14}	12*b* → 48*e*	0.8618(8)	0.9868(8)	0.2368(8)	2 (1)	0.25
R_B(%)		2.43				
R_P(%)		3.92				
R_{WP}(%)		5.07				
O/*M*		2.234				

The O_{14} atom has been splitted from the ideal 12*b* site (7/8, 0, 1/4) to a general site 48*e*.

The distribution of Ce and U on the seven cationic sites has been determined by successive steps, alternating with refinement of the *B* thermal factors. To limit the number of variables and possible correlation problems between the occupancy, the coordinates and the *B* factors of these cationic sites, the *B* thermal factors of

Table 2
Comparison of the atomic positions calculated in U_4O_9 using HADES code [9] and of the experimental values (present study) in $(U_{0.9}Ce_{0.1})_4O_{9-\delta}$

Atomic positions in $U_4O_{9-\delta}$ calculated with the HADES code [9]				Refined atomic positions in $(U_{0.9}Ce_{0.1})_4O_{9-\delta}$ with $a = 21.7484(1)$ Å (neutron diffraction)							
	x	y	z	x	Δx	y	Δy	z	Δz	B (Å^2)	τ
U_1	0	0	0	0.0026(4)	0.0026(4)	0.0026(4)	0.0026(4)	0.0026(4)	0.0026(4)	0.16(6)	
U_2	0.25	0	0.25	0.2516(8)	0.0016(8)	0	0	0.25	0	0.16(6)	
U_3	0.125	0.125	0.25	0.1249(5)	−0.0001(5)	0.1197(4)	−0.0053(4)	0.2484(6)	−0.0016(6)	0.16(6)	
U_4	0.003	0	0.25	−0.0020(6)	−0.0023(6)	0	0	0.25	0	0.62(9)	
U_5	0.875	0	0.121	0.8749(5)	−0.0001(5)	0.0031(4)	0.0031(4)	0.1198(4)	−0.0012(4)	0.62(9)	
U_6[Ce_6]	−0.004	0.121	0.371	−0.0053(5)	−0.0013(5)	0.1223(6)	0.0013(6)	0.3711(5)	−0.0001(5)	0.19(7)	0.72(6) [0.28(6)]
U_7[Ce_7]	−0.004	0.121	0.129	−0.0017(6)	0.0023(6)	0.1199(4)	−0.0011(4)	0.1308(5)	0.0018(5)	0.19(7)	0.79(6) [0.21(6)]
O_1	−0.03	0.094	0.25	−0.0287(7)	0.0013(7)	0.0935(7)	−0.0001(7)	0.2549(7)	0.0049(7)	1.7(2)	
O_2	−0.03	0	0.344	−0.0325(5)	−0.0025(5)	−0.0001(7)	−0.0001(7)	0.3424(6)	−0.0016(6)	0.60(2)	
O_3	0.875	0.094	0.334	0.8771(7)	0.0021(7)	0.0962(5)	0.0022(5)	0.3438(6)	0.0098(6)	0.60(2)	
O_4	0.0625	0.0625	0.0625	0.0608(8)	−0.0017(8)	0.0608(8)	0.0017(8)	0.0608(8)	−0.0017(8)	0.60(2)	
O_5	0.1875	0.1875	0.1875	0.1817(7)	−0.0058(7)	0.1817(7)	−0.0058(7)	0.1817(7)	−0.0058(7)	0.60(2)	
O_6	0.0625	0.1875	0.1875	0.0622(8)	−0.0003(8)	0.1835(8)	−0.0040(8)	0.1931(9)	0.0056(9)	0.60(2)	
O_7	0.072	0.0625	0.1875	0.0731(9)	0.0011(9)	0.0619(7)	−0.0006(7)	0.1879(7)	0.0004(7)	0.60(2)	
O_8	−0.0625	0.0625	0.052	−0.0635(8)	−0.0010(8)	0.0631(7)	−0.0006(7)	0.0554(7)	0.0034(7)	0.60(2)	
O_9	−0.0625	0.0625	0.4375	−0.0664(7)	−0.0039(7)	0.0594(7)	−0.0031(7)	0.4521(6)	0.0146(6)	0.60(2)	
O_{10}	−0.0625	0.197	0.1875	−0.0604(7)	0.0021(7)	0.1978(7)	0.0008(7)	0.1891(8)	0.0016(8)	0.60(2)	
O_{11}	−0.0625	0.197	0.3125	−0.0609(6)	0.0016(6)	0.1954(9)	−0.0016(9)	0.3145(7)	0.0020(7)	0.60(2)	
O_{12}	0.072	0.0625	0.3125	0.0688(7)	−0.0032(7)	0.0634(7)	0.0009(7)	0.3091(6)	−0.0034(6)	0.60(2)	
O_{13}	−0.0625	0.1875	0.4375	−0.0680(7)	−0.0055(7)	0.1849(7)	−0.0026(7)	0.4391(7)	0.0016(7)	0.60(2)	
O_{14}	−0.125	0	0.25	−0.1382(8)	−0.0132(8)	−0.0132(8)	0.0132(8)	0.2368(8)	−0.0132(8)	2(1)	0.25
R_B (%)		2.43									
R_P (%)		3.92									
R_{wp} (%)		5.07									

Δ: difference between the experimental and calculated coordinates.

the cations belonging to similar polyhedra, respectively UO_8 anionic cubes (for U_1, U_2 and U_3) (represented for U_1 in Fig. 2c), UO_8 square antiprisms (for U_4 and U_5) (represented for U_5 in Fig. 2a) and $(U,Ce)_{10}$ "centaur" polyhedra ($(U,Ce)_6$ and $(U,Ce)_7$) (represented for $(U,Ce)_7$ in Fig. 2b) have been respectively restricted to take the same value. The results are clear for cubic sites which are occupied only by uranium and for the "centaur" sites which contain significant amounts of cerium (resp. 28% and 21% mole for $(U,Ce)_6$ and $(U,Ce)_7$). The results are less clear for the square antiprisms inside which a weak proportion of Ce can be refined, but considering the limited accuracy of a powder refinement, this contribution has been neglected. The final refined Ce content is 9% mole, satisfactorily close to the nominal value ($\sim$10%). A weak proportion of Ce inside the square antiprisms is therefore possible. To verify that the U/Ce distribution is not biased by correlations on the cationic sites or by the imposed restraints on B thermal factors, a similar calculation has been performed on a $U_4O_{9-\delta}$ phase without cerium. For all the sites, the refined Ce content is always practically zero, which confirms the validity of the U/Ce distribution obtained for the Ce-substituted sample.

3.4. Anionic sites

Contrary to the cationic sites, a great part of the anionic ones are far from the ideal sites of the fluorite UO_2 subcell and their refinement does not cause any correlation problem. The refined B thermal factors of most anions (O_2–O_{13}) are very close and, in order to limit the number of variables, they have been constrained to take the same value. Only $B(O_1)$ and $B(O_{14})$ take higher values and are refined separately. A final Fourier-difference map shows that no other anionic sites are occupied. The main cation–anion distances are reported on Table 3a. The O_{14} site, firstly located, as in the ideal model, in the exact center of the cuboctahedral anionic void, appears in fact on the Fourier-difference maps as very diffuse and is refined with a very high B factor, in spite of a refined occupancy close to the nominal value for the site. Attempts to delocalize this anion to a more general site have been performed. The B factor decreases to a normal value but without significantly improve the R factor value. The most stable and logical solution selected in Table 1 corresponds to a statistical shift along 3-fold axes of the cuboctahedral cluster. It is then likely that the O_{14} anion, as in many homologous phases containing cuboctahedral clusters such as $Na_7Zr_6F_{31}$ and isotypic $M_7U_6F_{31}$ phases [11,12], is statistically shifted from the center of the cuboctahedral void in direction to a 3-fold axis and is only smoothly connected to the close cations. This is confirmed by a bond valence calculation of the anionic sites further discussed (Table 3b).

3.5. Composition of $(U_{0.9}Ce_{0.1})_4O_{9-\delta}$

The $(U_{0.9}Ce_{0.1})_4O_{9-\delta}$ phase is obtained with traces of U_3O_8 which suggests that the upper limit of anionic content ($\sim MO_{2.25}$) is obtained, by analogy to the Ce-free phase whose limits are close to $UO_{2.235}$–$UO_{2.245}$ at room temperature [3]. However, the composition resulting from the refined structure is $M_{64}O_{143}$ ($MO_{2.234}$) which corresponds to the lower limit of the $M_4O_{9-\delta}$ composition domain. Fourier-difference maps do not show any evidence for other weakly occupied anionic sites in this structure. Two possibilities exist:

- either the missing anions are distributed on several rather diffuse interstitial sites and cannot be detected on the basis of powder data only; the same problem exists for $U_4O_{9-\delta}$ and is yet unsolved;
- or the composition of $(U_{0.9}Ce_{0.1})_4O_{9-\delta}$ is perfectly stoichiometric and only corresponds to $(U_{0.9}Ce_{0.1})_{64}O_{143}$. Further experiments should be necessary to test this last hypothesis.

The composition $M_{64}O_{143}$ belongs to the M_mX_{2m+5} series [14–20] of anion-excess fluorite superstructures based on a three-dimensional ordered distribution of cuboctahedral structural units (Fig. 1; Table 4). The $M_{64}O_{143}$ structure, represented in Fig. 1 (for clarity, three superposed cationic layers only are shown), is a fractional $m = 21.33$ member of this series. Other fractional members are known with $m = 13.5$ ($Ln_{27}F_{64}$ (Ln = Sm, Eu, Yb) and the formulation M_mX_{2m+5} only means that each cuboctahedral cluster incorporates five excess anions during the transformation of a X_8 anionic cube into a X_{12+1} filled cuboctahedron. $M_{64}O_{143}$ is the member of this series with the smallest anionic excess ever described (except for $WTh_8Zr_{18}O_{53}F_4$ [21], an ordered intergrowth of cuboctahedral clusters and stabilized zirconia units of composition $MX_{2.11}$). It can be noted that Golubev [22] has proposed a new distribution of cuboctahedral cluster in adequation with the exact composition U_4O_9, but the space group and the lattice parameters proposed are not in agreement with our results.

3.6. Bond valence

A calculation of bond valences by Zachariasen's method [23,24] has been performed in order to check the accuracy of the atomic positions and to determine if the distribution of charges of the cations, supposed to be U^{4+}, Ce^{4+}, U^{5+} and/or U^{6+}, is ordered or disordered over the seven cationic sites. This method, implemented by Van den Berghe with small changes in a computer program [25] for the study of Cs uranates, is better adapted to U compounds presenting short uranyl bonds than the classical Brown's method [26]. For U^{4+}, both methods are quite equivalent. Zachariasen found that

Table 3
Interatomic distances d (Å): U–O and bond valences V, respectively, for (a) cations and (b) anions in the ordered phase $(U_{0.9}Ce_{0.1})_4O_{9-\delta}$

	d (Å)	V		d (Å)	V		d (Å)	V
(a)								
U1–O4	2.19(2)	0.773	U2–O6	2.35(2)	0.490	U3–O5	2.33(2)	0.518
U1–O5	2.67(2)	0.196	U2–O6	2.35(2)	0.490	U3–O6	2.29(2)	0.581
U1–O8	2.26(2)	0.633	U2–O10	2.21(2)	0.73	U3–O6	2.40(2)	0.424
U1–O8	2.26(2)	0.633	U2–O10	2.21(2)	0.73	U3–O7	2.14(2)	0.892
U1–O8	2.26(2)	0.633	U2–O11	2.24(2)	0.670	U3–O9	2.27(2)	0.615
U1–O9	2.24(2)	0.670	U2–O11	2.24(2)	0.670	U3–O10	2.23(2)	0.690
U1–O9	2.24(2)	0.670	U2–O13	2.42(2)	0.401	U3–O12	2.18(2)	0.796
U1–O9	2.24(2)	0.670	U2–O13	2.42(2)	0.401	U3–O13	2.32(2)	0.533
d_{av}; $\mathbf{V_{(O)}}$	⟨2.30⟩	4.88	d_{av}; $\mathbf{V_{(O)}}$	⟨2.31⟩	4.58	d_{av}; $\mathbf{V_{(O)}}$	⟨2.27⟩	5.05
U4–O1	2.11(2)	0.972	U5–O1	2.23(2)	0.690			
U4–O1	2.11(2)	0.972	U5–O2	2.18(1)	0.796			
U4–O2	2.11(1)	0.972	U5–O3	2.30(1)	0.565			
U4–O2	2.11(1)	0.972	U5–O3	2.11(1)	0.972			
U4–O7	2.51(2)	0.310	U5–O8	2.34(2)	0.504			
U4–O7	2.51(2)	0.310	U5–O9	2.43(2)	0.390			
U4–O12	2.43(2)	0.390	U5–O10	2.46(2)	0.358			
U4–O12	2.43(2)	0.390	U5–O11	2.39(2)	0.437			
U4–O14	2.42(2)	0.390	U5–O14	2.58(2)	0.254			
d_{av}; $\mathbf{V_{(O)}}$	⟨2.30⟩	5.69	d_{av}; $\mathbf{V_{(O)}}$	⟨2.33⟩	4.96			
U6–O1	2.65(2)	0.228	U7–O1	2.82(2)	0.145			
U6–O2	2.79(2)	0.155	U7–O2	2.76(2)	0.172			
U6–O3	2.68(2)	0.209	U7–O3	2.83(2)	0.14			
U6–O8	2.33(2)	0.543	U7–O4	2.41(2)	0.438			
U6–O9	2.59(2)	0.266	U7–O6	2.38(2)	0.475			
U6–O11	2.35(2)	0.523	U7–O7	2.40(2)	0.45			
U6–O12	2.40(2)	0.45	U7–O7	2.38(2)	0.475			
U6–O13	2.46(2)	0.383	U7–O8	2.46(2)	0.386			
U6–O13	2.43(2)	0.416	U7–O10	2.47(2)	0.371			
U6–O13	2.40(2)	0.456	U7–O12	2.45(2)	0.393			
d_{av}; $\mathbf{V_{(O)}}$	⟨2.51⟩	3.63	d_{av}; $\mathbf{V_{(O)}}$	⟨2.54⟩	3.45			
(b)								
O1–U4	2.11(2)	0.972	O2–U4	2.11(1)	0.972	O3–U5	2.30(1)	0.565
O1–U5	2.24(2)	0.690	O2–U5	2.18(1)	0.796	O3–U5	2.11(1)	0.972
O1–U6	2.65(2)	0.228	O2–U6	2.79(2)	0.155	O3–U6	2.68(2)	0.209
O1–U7	2.82(2)	0.145	O2–U7	2.76(2)	0.172	O3–U7	2.83(2)	0.140
d_{av}; $\mathbf{V_{(O)}}$	⟨2.46⟩	2.04	d_{av}; $\mathbf{V_{(O)}}$	⟨2.46⟩	2.10	d_{av}; $\mathbf{V_{(O)}}$	⟨2.48⟩	1.89
O4–U1	2.19(2)	0.773	O5–U1	2.67(2)	0.196	O6–U2	2.35(2)	0.490
O4–U7	2.41(2)	0.438	O5–U3	2.33(2)	0.518	O6–U3	2.29(2)	0.581
O4–U7	2.41(2)	0.438	O5–U3	2.33(2)	0.518	O6–U3	2.40(2)	0.424
O4–U7	2.41(2)	0.438	O5–U3	2.33(2)	0.518	O6–U7	2.38(2)	0.475
d_{av}; $\mathbf{V_{(O)}}$	⟨2.36⟩	2.09	d_{av}; $\mathbf{V_{(O)}}$	⟨2.42⟩	1.75	d_{av}; $\mathbf{V_{(O)}}$	⟨2.36⟩	1.97
O7–U3	2.14(2)	0.892	O8–U1	2.26(2)	0.633	O9–U1	2.24(2)	0.670
O7–U4	2.51(2)	0.310	O8–U5	2.34(2)	0.504	O9–U3	2.27(2)	0.615
O7–U7	2.40(2)	0.450	O8–U6	2.33(2)	0.536	O9–U5	2.44(2)	0.390
O7–U7	2.38(2)	0.475	O8–U7	2.46(2)	0.386	O9–U6	2.60(2)	0.266
d_{av}; $\mathbf{V_{(O)}}$	⟨2.36⟩	2.13	d_{av}; $\mathbf{V_{(O)}}$	⟨2.35⟩	2.06	d_{av}; $\mathbf{V_{(O)}}$	⟨2.39⟩	1.94
O10–U2	2.21(2)	0.730	O11–U2	2.24(2)	0.670	O12–U3	2.18(2)	0.796
O10–U3	2.23(2)	0.690	O11–U5	2.39(2)	0.437	O12–U4	2.43(2)	0.390
O10–U5	2.46(2)	0.358	O11–U6	2.35(2)	0.523	O12–U6	2.46(2)	0.383
O10–U7	2.47(2)	0.371	O11–U6	2.40(2)	0.450	O12–U7	2.45(2)	0.393
d_{av}; $\mathbf{V_{(O)}}$	⟨2.34⟩	2.15	d_{av}; $\mathbf{V_{(O)}}$	⟨2.35⟩	2.08	d_{av}; $\mathbf{V_{(O)}}$	⟨2.38⟩	1.96
O13–U2	2.42(2)	0.401	O14–U4	2.99(2)	0.091			
O13–U3	2.32(2)	0.533	O14–U4	2.42(2)	0.401			
O13–U6	2.43(2)	0.416	O14–U5	2.58(2)	0.254			
O13–U6	2.4(2)	0.456	O14–U5	2.57(2)	0.286			
d_{av}; $\mathbf{V_{(O)}}$	⟨2.39⟩	1.81	d_{av}; $\mathbf{V_{(O)}}$	⟨2.64⟩	1.08			

The U_1, U_2, U_3 sites correspond to cubic environments, U_4, U_5 to square antiprisms, U_6 and U_7 to "centaur" polyhedra (the Ce content on these last sites is neglected). The bond valences have been calculated with $R_0 = 2.112$ Å for U^{4+}, 2.100 Å for U^{5+} and 2.083 Å for U^{6+} ($B = 0.35$). Using Zachariasen's method [24].

Table 4
M_mX_{2m+5} series of ordered anion-excess fluorite superstructures containing cuboctahedral clusters

m	Composition M_mX_{2m+5}	X/M ratio	Examples	Ref.
13	$M_{13}X_{31}$	2.38_4	$Na_7Zr_6F_{31}$, $Ca_8Y_5F_{31}$, $M_7U_6F_{31}$	[11,12,15,16]
13+14 (13.5)	$M_{27}X_{64}$	2.37_0	$Ln_{27}F_{64}$ (Ln=Sm, Eu, Yb)	[15]
14	$M_{14}X_{33}$	2.35_7	$Ca_9Y_5F_{33}$, $Ln_{14}F_{33}$ (Ln=Sm, Eu, Yb)	[15,16]
15	$M_{15}X_{35}$	2.33_3	Ca_2LnF_7 (Ln=Lu–Ho, Y)	[15,16,17,19]
			Sr_2LnF_7 (Ln=Sm–Lu)	[18]
			Ln_3F_7 (Ln=Sm, Eu, Yb)	[15]
			U_3O_7	[20]
19	$M_{19}F_{43}$	2.26_3	$Ca_{14}Y_5F_{43}$ (tveitit)	[14]
20	$M_{20}X_{45}$	2.25		
21	$M_{21}X_{47}$	2.23_8		
21+21+22 (21.33)	$M_{64}X_{143}$	2.23_4	$U_{64}O_{143}$	[9,10] present work
22	$M_{22}X_{49}$	2.22_7		

the logarithmic form of the bond valence curve:

$$R(s) = R_0 - B\ln s, \quad \text{with } B = AR_0 \tag{2}$$

gives good agreement with experiment for many oxides and halides of d and f elements. s is the bond strength between two atoms, R_0 is the bond length for unit bond strength, B and A are constants. R_0 distances are directly determined for pairs of atoms from crystal structures. The constant value of 0.37 is generally retained for B but more specific values can be used for R_0 and B in particular in the compounds with f-elements because of their atypical bonding characteristics. For the present phase, a value of 0.35 is used for B except when $s>1$ where $B = 0.35 + 0.12(s-1)$. In the last case, the actual value of s can be calculated iteratively.

It must be noted that some approximations and limitations cannot be avoided: the R_0 value for U^{5+} (2.10 Å) is interpolated between those of U^{4+} (2.112 Å) and U^{6+} (2.083 Å); the experimental M–O distances can be imprecise or averaged if cations of slightly different size and charge statistically occupy the same cationic site (e.g., U^{4+}/Ce^{4+} or $U^{4+}/U^{5+}/U^{6+}$).

Tables 3a and b gather the calculated bond valences respectively for cationic and anionic sites.

All anionic sites, except O_{14}, have calculated valences ranging between 1.75 and 2.15 which means that these anions are well localized, in spite of the use of powder data and the limitations above discussed. The bond valence of the O_{14} site, rather imprecise owing to the diffuse character of the site, is much lower: $V \sim 1$, which confirms the weakly bonded character of this anion trapped inside the cuboctahedral void.

The cationic sites present significant differences: the 10-fold coordinated sites (centaur polyhedra) are undoubtedly occupied by tetravalent U and Ce and the U_4 and U_5 sites probably contain U^{5+} and/or U^{6+} cations in UO_8 square antiprisms. The U_1, U_2 and U_3 sites (cubic coordination) are likely occupied by a disordered mixture of U^{4+} and U^{5+} (and/or U^{6+}). Therefore, a preferential charge ordering is likely present in $(U_{0.9}Ce_{0.1})_{64}O_{143}$. These conclusions are in agreement with the cationic ordering generally observed in other anion-excess fluorite superstructures containing cuboctahedral clusters: the "centaur" polyhedra are occupied by high size, low charge cations (alkaline, alkaline-earth, Pb^{2+}, etc.), the square antiprisms by low or medium size, high charge cations (Ln^{3+}, Zr^{4+}, etc.) and the other sites deriving from cubes are often fully or partly disordered (e.g., mixtures of Ca^{2+} and Lu^{3+} in Ca_2LuF_7 [19]). It could be significant to note that the complete replacement of U^{4+} by Ce^{4+} on the $(U,Ce)_6$ and $(U,Ce)_7$ "centaur" sites corresponds to 37.5% mole Ce^{4+}, not far from the experimental limit (34%) proposed by Markin [1].

4. Conclusion

Among the various anion-excess fluorite superstructures already described, the $(U,Ce)_4O_{9-\delta}$ type, now more conveniently called $(U,Ce)_{64}O_{143+\delta}$ type, presents unique features. It is the only example of an ordered fluorite phase based on the association of cuboctahedral structural units containing such a low anionic excess ($MO_{2.234}$). Its stability likely results from rather slight cationic shifts from the ideal fluorite positions and mainly from fast electron exchanges between U^{4+}, U^{5+} and/or U^{6+}. These fast exchanges, even at low temperature, make possible a distribution of U charges on the cationic sites which allows a convenient local charge equilibrium favoring the formation and the ordering of the anionic cuboctahedral clusters easily formed by anionic diffusion. This structure type accepts the substitution of U^{4+} by Ce^{4+} on the cationic sites occupied by the "centaur" polyhedra without loosing the long-range ordering of the cuboctahedral structural units.

References

[1] T.L. Markin, R.S. Street, E.C. Crouch, J. Inorg. Nucl. Chem. 32 (1970) 59.
[2] H. Blank, C. Ronchi, Acta Crystallogr. A 24 (1968) 657.
[3] W. Van Lierde, J. Pelsmaekers, A. Lecocq-Robert, J. Nucl. Mater. 37 (1970) 276.
[4] B. Belbeoch, J.C. Boivineau, Bull. Soc. Fr. Mineral. Crystallogr. XC (1967) 558.
[5] T. Ishii, K. Naito, K. Oshima, Y. Hamaguchi, J. Phys. Chem. Solids 32 (1971) 235.
[6] T. Matsui, K. Naito, J. Nucl. Mater. 56 (1975) 327.
[7] B. Belbeoch, C. Piekarski, P. Perio, Acta Crystallogr. 14 (1961) 837.
[8] J.P. Lauriat, G. Chevrier, J.X. Boucherle, J. Solid State Chem. 80 (1989) 80.
[9] D.J.M. Bevan, I.E. Grey, B.T.M. Willis, J. Solid State Chem. 61 (1986) 1.
[10] B.T.M. Willis, Advances in Ceramics, Vol. 23: Non-stoichiometric compounds, 1987, American Ceramic Society, p. 711.
[11] J.H. Burns, R.D. Ellison, H.A. Levy, Acta Crystallogr. B 24 (1968) 230.
[12] R.A. Penneman, R.R. Ryan, A. Rosenzweig, Structure and Bonding, Vol. 13, Springer, Berlin, 1973, p. 1.
[13] J. Rodriguez-Carvajal, L.L.B, unpublished program, 1994.
[14] D.J.M. Bevan, J. Strähle, O. Greis, J. Solid State Chem. 44 (1982) 75.
[15] O. Greis, Proceedings of the 14th Rare Earth Conference, Vol. 2, Fargo, USA, June 25–29, 1979, p. 167.
[16] W. Gettmann, O. Greis, J. Solid State Chem. 26 (1978) 255.
[17] D.J.M. Bevan, et al., Eur. J. Solid State Inorg. Chem. 25 (1988) 509 (3 papers).
[18] O. Greis, M.S.R. Cader, J. Less-Common Met. 118 (1986) 21.
[19] J.P. Laval, A. Abaouz, B. Frit, A. Le Bail, J. Solid State Chem. 85 (1990) 133.
[20] F. Garrido, R.M. Ibberson, L. Nowicki, B.T.M. Willis, J. Nucl. Mater. 322 (2003) 87.
[21] J.P. Laval, A. Taoudi, J. Solid State Chem. 115 (1995) 283.
[22] A.M. Golubev, Koord. Khim. 18 (12) (1992) 1232.
[23] W.H. Zachariasen, J. Less-Common Met. 62 (1978) 1.
[24] W.H. Zachariasen, R.A. Penneman, J. Less-Common Met. 69 (1980) 369.
[25] S. Van den Berghe, M. Verwerft, J.P. Laval, B. Gaudreau, P.G. Allen, A. Van Wyngarden, J. Solid State Chem. 166 (2002) 320.
[26] I.D. Brown, in: M. O'Keeffe, A. Navrotsky (Eds.), Structure and Bonding in Crystals, Academic Press, New York, 1981.